



UNITED NATIONS
UNIVERSITY

UNU-GTP

Geothermal Training Programme

Orkustofnun, Grensasvegur 9,
IS-108 Reykjavik, Iceland

Reports 2015
Number 34

EVALUATION OF FACTORS CONTROLLING THE CONCENTRATION OF NON-CONDENSIBLE GASES AND THEIR POSSIBLE IMPACT ON THE PERFORMANCE OF WELLS IN OLKARIA, KENYA

Ruth Nelima Wamalwa

Kenya Electricity Generating Company - KenGen

P.O. Box 785-20117

Naivasha

KENYA

wamalwarn2000@gmail.com, rwamalwa@kengen.co.ke

ABSTRACT

The Olkaria geothermal field is located in the Kenyan Rift valley about 120 km from Nairobi. Development of geothermal resources in a high temperature field in the Olkaria area started in the early 1950s. In the following years numerous developments have been made with additional power plants being installed. These include a binary plant at Olkaria South West (Olkaria III) in 2000, a condensing plant at Olkaria North East (Olkaria II) in 2003, another binary plant at Olkaria North West (Oserian) in 2004 and finally two more condensing plants in the year 2014 within the East production field (EPF) and Olkaria Domes (OD) areas. The total generation from the field is about 730 Mw.

In this study samples from four producing wells located in three fields in the Olkaria geothermal area (OW-44 in the Olkaria East, OW-724A in the Olkaria North East and OW-914, and OW-915 in the Olkaria Domes field) were studied. The chemical analysis was carried out using SOLVEQ. The equilibrium state of the system was determined, the reservoir temperatures and the total moles were run through the CHILLER program. The CHILLER runs analysed the processes that have been proven to be occurring in the Olkaria field, i.e. boiling and condensing processes, fluid-fluid mixing rocks and titration resulting from water-rock interaction. The effects on gas evolution were evaluated based on the recalculated gas pressures.

The results indicate that the gas species are not in equilibrium with the mineral assemblages. The CHILLER evaluation shows boiling as the major process leading to evolution of gases. Well OW-44 had the smallest gas concentrations resulting from the reservoir processes in question due to degassing and near surface boiling. Gas breakout is most likely in well OW-914 and least likely in well OW-44. The study proposes different reservoir management strategies for the different parts of the Olkaria geothermal field. The first would be by increasing hot reinjection in the eastern sector around well OW-44. In the part of the reservoir around well OW-914, the wells should be operated at a minimum flow rate, or chemical inhibitors to prevent calcite scaling could be used.

1. INTRODUCTION

Evaluation of gas concentrations in Olkaria geothermal field revealed that on average gases are highest in the Domes, intermediate in Northeast production field and lowest in East production field (West JEC, 2009). West JEC (2009) considers three possible causes for the variations: i) CO₂ is accumulated in the water at great depth in the Northeast production field and Domes waters as a result of volcanic degassing below these areas, this process is less dominant in the East production field; ii) CO₂ addition at depth is similar in all three areas but water of the East production field loose CO₂ during the boiling process in the reservoir which escapes to fumaroles west and south of the East production field iii) cap-rock conditions in the Northeast production field and Domes are more restrictive than in the East production field, leading to more entrapment of CO₂ that has been released by boiling at shallower depths. Gases, in particular CO₂, H₂S, H₂, and CH₄, are natural components of volcanic geothermal systems such as Olkaria (Kenya), Mahanagdong (Philippines) and Nesjavellir, Hellisheidi and Krafla in Iceland (Arnórsson et al., 2010; Angcoy, 2010).

The gas concentration in unexploited systems is generally controlled by temperature dependent equilibria with various mineral buffers (Giroud and Arnórsson, 2005). Giroud and Arnórsson, (2005) also stated that for geothermal systems with average reservoir temperatures between 230-300°C the CO₂ buffer is considered to be clinozoisite, prehnite, quartz, and calcite whereas that for H₂S the main buffer minerals are pyrite, pyrrhotite, epidote, and prehnite. In highly saline waters, the H₂S mineral buffer consists of pyrite, magnetite and hematite. The gas ratios such as the H₂S/H₂ activity ratio correspond closely to the equilibrium of the mineral pairs pyrite/pyrrhotite and pyrite/magnetite which are generally undersaturated with respect to the individual minerals. These findings agree with the study of the Olkaria field by Karingithi (2002) which found that the activity of aqueous H₂ and H₂S gases generally corresponds closely to the equilibrium of the mineral buffer pyrite, pyrrhotite, and magnetite. The activities of these two gases also correspond closely to the equilibrium of the mineral buffer pyrrhotite, prehnite, epidote, and pyrite. The H₂S/H₂ activity ratio corresponds closely to the equilibrium of the mineral pairs pyrite/pyrrhotite and pyrite/magnetite.

The concentration of gases in exploited geothermal fields are higher than of the parent fluid (Akin et al., 2015). The value is frequently in the range of 50-300 and 2-20 mmol/kg of steam for CO₂ and H₂S respectively (Giroud and Arnórsson, 2005). The variation is dependent on the concentration in the geothermal parent fluid, the steam fraction, the steam separation pressure, and the boiling processes. According to Giroud and Arnórsson, (2005), long-term utilization of geothermal reservoirs can lead to a decline of CO₂ and H₂S concentrations in the steam. This decline may be caused by recharge of cold water into producing aquifers and/or progressive boiling of water retained in the aquifer by capillary forces. Enhanced boiling, which is a consequence of reservoir pressure draw down and steam separation during lateral flow into production wells, may cause the well discharge to become depleted of gas. In case of a boiling reservoir, the gas concentrations tend to be higher compared to concentrations at a particular temperature. The formation of steam caps in the reservoir is observed more frequently and/or an enhance in fumarolic activity. Karingithi (2002) also notes that gas samples from marginal wells whose discharge fluid are mixed with non-geothermal fluid show low H₂ and H₂S values with respect to the equilibrium with the buffer mentioned above.

The gases are among the factors that affect the reservoir pressure in the deep liquid-dominated geothermal reservoirs (Haizlip et al., 2012). Haizlip et al. (2012) further added that under static conditions, pressure in most producing aquifers around the world ranges between 130 to 230 bars at depths between 1700 to 2800 m. The temperatures at this depth range from 219 to 242°C. The effect of the gas pressures on well performance is evaluated by the gas breakout pressure i.e. the pressure below which the fluids begin to transform into two phases. According to Haizlip et al. (2012) gas breakout pressure is the sum of the gas pressure and water pressure at the reservoir temperature. Due to pressure drop, thermal fluids start to boil when rising in the wellbore and CO₂ is released. In bicarbonate type of waters, the fluid becomes saturated with calcite due to a reaction of CO₂ and calcium.

For an exploited field such as the Olkaria area, changes in the gas content of well discharges over time help providing valuable information about the response of the reservoir to the production load (Karingithi, 2002). These changes are a consequence of various processes such as cold recharge resulting to fluid-fluid mixing, volcanic degassing, and enhanced boiling (Gudmundsson and Arnórsson, 2002; Ármannsson, 2003). In this study, an evaluation of reaction processes controlling the concentration of prevalent reactive gases CO_2 , H_2S , H_2 , CH_4 , and N_2 in Olkaria well discharges, is made. The procedure involves the calculation of the equilibrium state between fluids and rocks using the software package SOLVEQ followed by the determination of reaction processes in aqueous-mineral-gas systems using the software package CHILLER (Reed et al., 2012a, b). The software packages SOLVEQ and CHILLER, have been chosen because of their applicability for studying multiphase systems as well as undergoing boiling and mixing processes (Bienkowski et al., 2003). This is relevant for the long-term release of gases from geothermal power plants and makes it interesting for predicting a possible decline in gas emissions. Eventually the results are compared to the measured pressures through the downhole temperature and pressure surveys to determine if there are chances of gas breakout occurrence.

2. GENERAL SETTING OF THE STUDY AREA

The Olkaria Geothermal area is located within the Olkaria central volcanic complex in the central sector of the Kenyan Rift Valley. The complex is located south of Lake Naivasha, approximately 120 km from the capital Nairobi. It is bordered by other geothermal prospect areas like Suswa, Longonot, and Eburru (Figure 1).

The Olkaria geothermal area covers approximately 140 km² and is divided into seven fields: Olkaria East, Olkaria Northeast, Olkaria Central, Olkaria Northwest, Olkaria Southwest, Olkaria Southeast, and Olkaria Domes (Figure 2). The fields are in different stages of development. Olkaria East, Olkaria Northeast and Olkaria Southwest are fully explored while Olkaria-Domes is the most recent of them where exploitation started in 2014. Olkaria Southwest is yet to be developed.

The Olkaria East Field is located on the East of the Olkaria hill (Figure 3) and has been under steam exploitation since 1985. The Olkaria 1 power plant is served by 31 wells connected to the steam gathering system. At the end of 2014, the steam of only 22 wells was utilized. 9 wells had become non-commercial producers because of a decline in output. Two of these wells, OW-6 and OW-3, are used as reinjection wells whereas OW-11 was

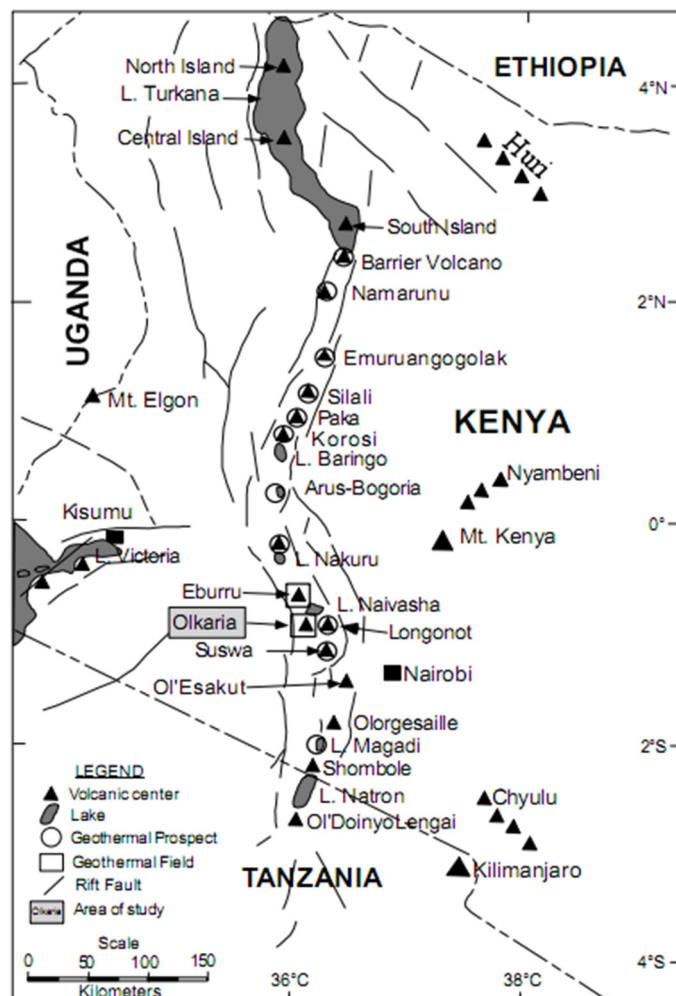


FIGURE 1: Map of the Kenya rift showing the location of Olkaria geothermal field and other Quaternary volcanoes along the rift valley (Lagat, 2005)

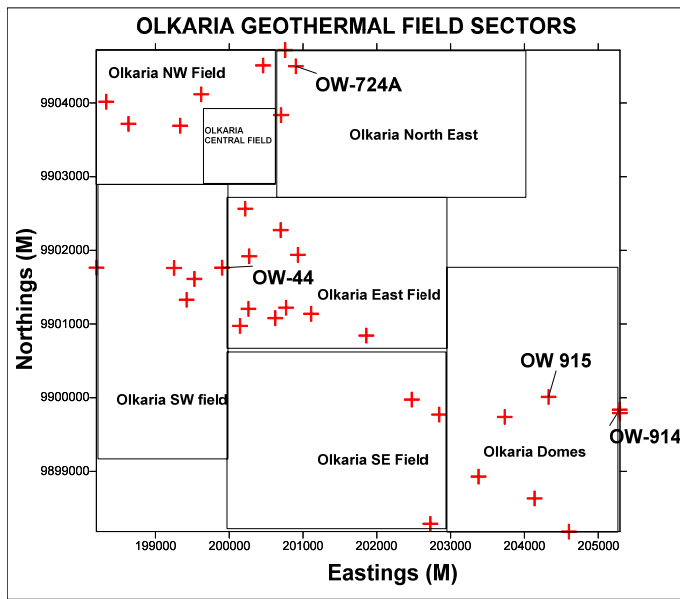


FIGURE 2: Geothermal fields within the Greater Olkaria geothermal area (KenGen, 1999); the red crosses indicate the location of wells; labelled wells are the ones used in this study

recently commissioned to take low pressure (LP) brine from OW-2. The field also hosts newly drilled wells like OW-35, OW-36A, OW-37A, OW-38, OW-38A, OW-41, OW-42A, OW-44, OW-44A, and OW-44B for the Olkaria1 unit IV and V power plant. This power plant was commissioned in October, 2014. OW-37A, OW-43, and OW-43A are connected to wellhead generators.

The Olkaria North East has been used for power generation since October 2003. It has a total of 20 wells that are connected to the steam gathering system. Of the twenty, 6 wells (OW-709, OW-710, OW-712, OW-713, OW-718, and OW-721) have individual separators while the other 14 wells (OW-701, OW-727, OW-705, OW-725, OW-706, OW-711, OW-707, OW-715, OW-714, OW-716, OW-719, OW-726, OW-720, and OW-728) share separators. Four wells are used for hot re-injection (OW-R2, OW-R3, OW-703, and OW-708). Wells OW-704, OW-717, OW-723, and OW-724 are non-producers and are currently used for pressure monitoring (Figure 2).

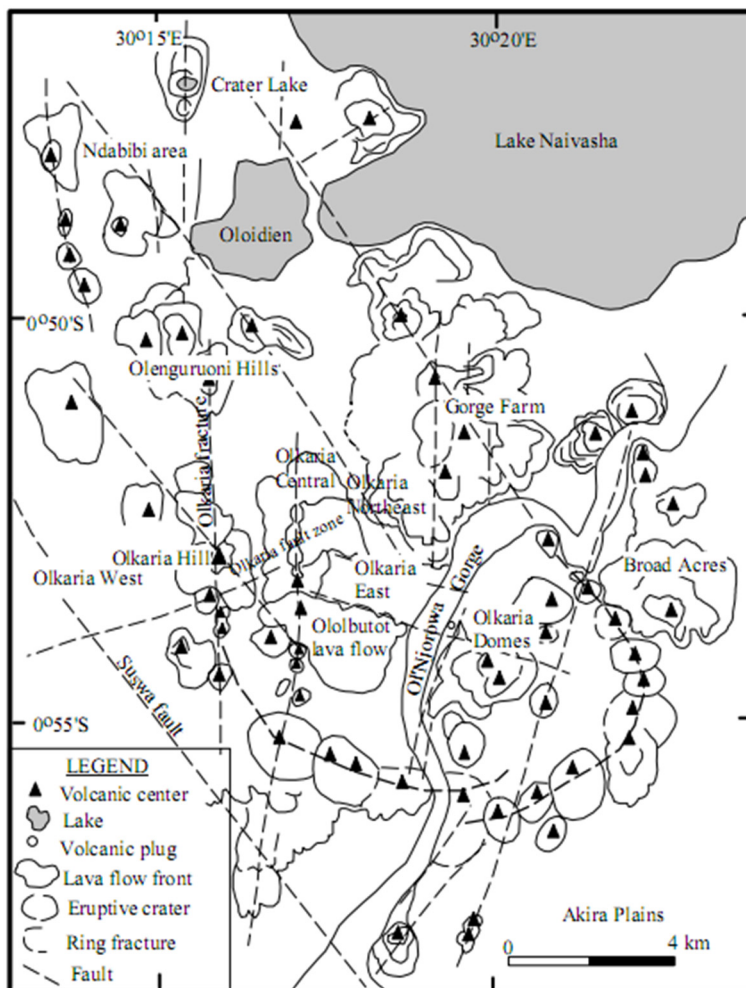


FIGURE 3: Volcano-tectonic map of the Greater Olkaria volcanic complex (modified after Clarke et al., 1990)

Olkaria-Domes field lies to the west of Longonot Volcano and on the SE of the Olkaria hill (Figure 3). It was the last of the seven sectors at which test drillings for exploration purposes were carried out. Three deep exploration wells were drilled in 1998 and 1999. Drilling was halted for about eight years due to shortage of funding but resumed in June 2007. This led to realization of a 140 MWe power plant commissioned in October, 2014 using wells OW-910, OW-910A, OW-910B, OW-908, OW-908A, OW-908B, OW-909, OW-915, OW-915A, OW-915B, OW-916, and OW-912.

2.1 Geological features and physical characteristics of the reservoir

2.1.1 Geology of Olkaria volcanic complex

Olkaria volcanic complex does not have a clear caldera association (Naylor, 1972; Virkir, 1980; Clarke et al., 1990; Mungania, 1992). However, Lagat et al., (2005) concluded that the presence of a ring of domes in the east, south and southwest can be used to infer the presence of a buried caldera. The downhole geology in geothermal wells in Olkaria field has helped to reveal the lithostratigraphy of the area (Omenda, 2000). In this study, the regional geology has been divided into six main lithostratigraphy groups: proterozoic “basement” formations, pre-Mau volcanics, Mau tuffs, plateau trachytes, Olkaria basalt and Upper Olkaria volcanics. The basement rocks contain Proterozoic gneisses of amphibolite facies-grade, schists, marbles, and quartzites of the Mozambique group (Shackleton, 1986; Smith and Mosley, 1993). The Mau tuffs are the oldest rocks that outcrop on the surface in the Olkaria area. Omenda (1994, 2000) concluded that this might be the surface manifestation of an east dipping high angle normal fault that is cutting through Olkaria Hill. The Upper Olkaria volcanics are overlain by Olkaria basalt in the area to the east of Olkaria Hill while the formation is absent west of it. This formation consists of basalt flows, minor pyroclastics and trachytes and varies in thickness from 100 m to 500 m (Omenda, 2000). The Upper Olkaria formations comprise of mainly lavas and ashes from Suswa and Longonot volcanoes (Thompson et al., 1963; Ogozo-Odongo, 1986; Clarke et al., 1990; Omenda, 2000).

2.1.2 Structural setting of the Olkaria volcanic complex

Structures in the Olkaria geothermal area include a ring structure, the Ol’Njorowa gorge, the Gorge Farm fault, the ENE-WSW Olkaria fault and NW-SE trending faults (Figure 3). Faults are prominent in the East, Northeast and West Olkaria fields unlike in the Olkaria Domes area where they are most likely covered by thick pyroclastic rocks (Clarke et al., 1990). The NW-SE trending faults are considered to be the oldest and are associated with the development of the rift and the presence of hot chloride-rich fluids. An exception is the Gorge farm fault, which bounds the geothermal fields in the north eastern part and extends to the Olkaria Domes area. The most recent structures are the NNE-SSW faults. They are thought to be young and carry cold fluids low in chlorite.

Dike swarms exposed in the Ol’Njorowa gorge trend in a NNE direction confirming the reactivation of recent faults of similar orientation. The development of the Ol’Njorowa gorge is thought to have been initiated by faulting along the orientation of the gorge but the feature as it appears today resulted from a catastrophic outflow of Lake Naivasha during its high stands (Clarke et al., 1990). The volcanic plugs (necks) and felsic dikes along the gorge are another evidence that the fault controls the development of this feature. Subsurface faults have been encountered in most Olkaria wells (KenGen, 1999). They are witnessed mostly in wells where drilling problems were encountered when these faults were dissected. The problems included collapse, and loss of drilling fluids and cement. The cuttings recovered from these zones are mainly fault breccias.

3. RESERVOIR CHARACTERISTICS

3.1 Reservoir pressure and temperature characteristics

Studies on the temperature and pressure distribution in the Olkaria field indicate that fluid movement in the geothermal system is tectonically controlled (Ofwona, 2002). The reservoir temperatures reach as high as 380°C at 3400 metres depth in well OW-49 in Olkaria East. The Olkaria East and North East consist of a two-phase reservoir (reservoir with a steam and water mixture feed zone) at least to the depth that is penetrated by the deepest wells. On the other hand, the Olkaria Domes consist of a liquid-dominated reservoir without a steam cap (Ambusso and Ouma, 1991; KenGen 1999).

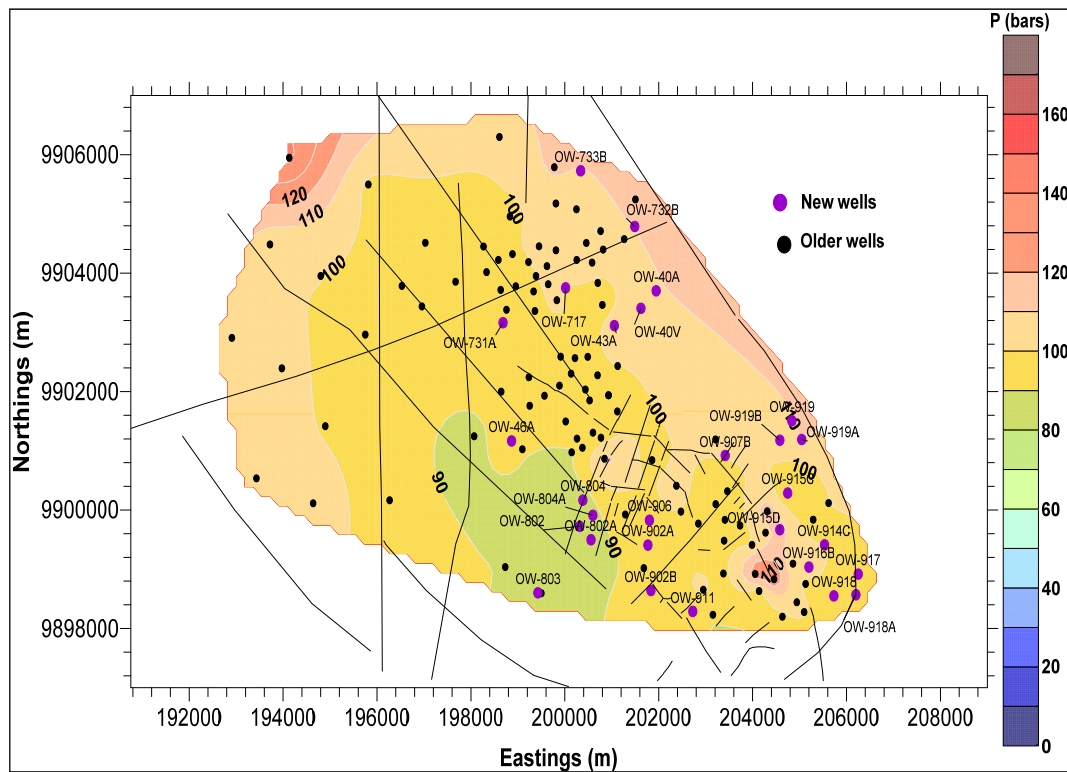


FIGURE 4: Measured pressure variations for the Olkaria geothermal field

Pressure decreases both eastwards and westwards from respective peaks towards Olkaria Central (Figure 4). Within the Olkaria Central and North East, pressures decline southwards towards both well OW-401 and Olkaria East (Ouma, 1999).

As shown in the profiles in Figure 5, well OW-44 was drilled to 3000 m in early 2011. It has a high injectivity index of 164 l pm/bar and downhole temperatures of about 300°C. Major feed zones are observed at around 760 m and 2250 m while minor ones have been localized at 1500 and 1750 m depth. Well OW-724A just like well OW-44 was drilled to a depth of 3000 m in early 2012. It has a slightly higher injectivity index of about 180 l pm/bar. The major feed zone in this well is at 1800 m and minor ones are observed at 1400, 1750, 2000, and 2550 m depths as seen in the heat up temperature profiles. The pressure profiles indicate that the water rest level was at 550 m depth prior to the injection. A pivot point has been observed in around 1800 m depth hence the major feed zone is in around 1800 m depth.

The temperature profile taken at well OW-915 in the Olkaria Domes field indicates minor feed zone between 1200 m and 1500 m and a major feed zone at 2300 m metres depth. The pre-injection data shows a water rest level at approximately 300 m depth. The well has with 145 l pm/bar a low injectivity index compared to wells OW-44 and OW-724A.

3.2 Reservoir fluid chemistry

The Olkaria wells discharge fluids with enthalpy ranging from 1000 kJ/kg to 2750 kJ/kg (Karingithi, 2002). Wells in the eastern production field have excess discharge enthalpy. This implies that the enthalpy of discharged fluid is higher than that of steam-saturated water at the respective aquifer temperatures. The water discharged from wells in the Olkaria field is poor in dissolved solids compared to fluids from most other high-temperature geothermal fields in the world with chloride concentrations in liquid ranging between 50 and 1100 ppm (Karingithi, 2000). The water of wells in Olkaria East and Northeast (Figure 2) tends to be highest in chloride with about 1000 ppm. According to Karingithi

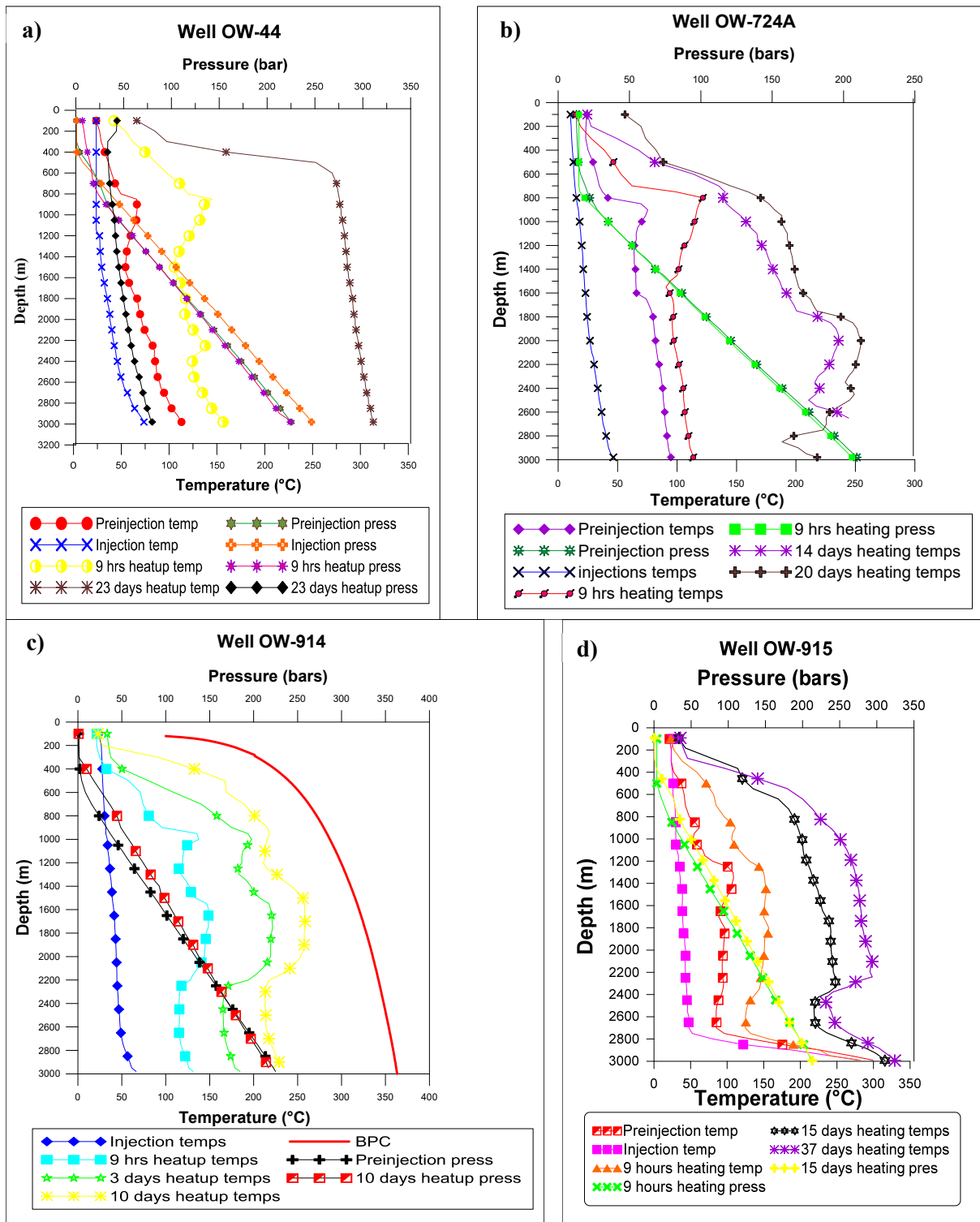


FIGURE 5: Downhole temperature and pressure profiles for wells OW-44 (a), OW-724 (b), OW-914 (c), and OW-915 (d) BPC stands for boiling point curve

(2002) the high chloride content could be as a result of up-flow of high-temperature geothermal fluid, although progressive boiling by heat flow from the rock may also be a contributing factor.

A study by Wambugu (1995) found that in Olkaria West field the chloride concentrations are quite low with about 350 ppm except for well OW-305 which discharges water similar to that of the wells in the Olkaria East and Olkaria Northeast fields. Well OW-305 is therefore thought to be tapping of the up-

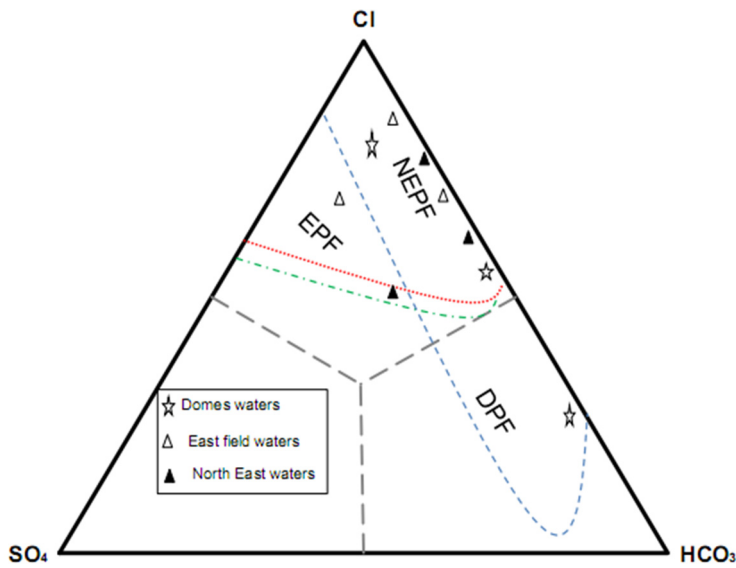


FIGURE 6: Cl-SO₄-HCO₃ ternary diagram for the Olkaria geothermal field. FPF stands for East production field, NEPF for North East production field while DPF for Domes production field

geothermal fluid and a subsequent reaction between the carbonic acid and minerals of the rock leading to evolution of CO₂ gas.

flow fluid for Olkaria West field. The relative abundance of chloride, sulfate and bicarbonate show that wells in the Olkaria East production field and in Olkaria North East discharge sodium-chloride type water while the Olkaria Domes fields discharge a mixture of chloride and bicarbonate end-member water (Figure 6) (KenGen, 2014). The liquid from Olkaria wells is slightly to moderately alkaline (pH 8.1-9.9 as measured at 20°C) and is relatively high in bicarbonate (Wambugu, 1995). The bicarbonate concentration is in the range of 90-13000 ppm with the highest carbon dioxide content found in the Olkaria West field followed by the Olkaria Domes. Wambugu (1995) added that this could be a consequence of CO₂ supply to the

3.3 Geochemical conceptual model

The geochemical data identifies upflow zones in the areas around wells OW-701, OW-711, and OW-705 in the Olkaria North East field, around wells OW-38, OW-32, OW-35A, and OW-39A in the Olkaria East field and in the Olkaria Domes area in wells OW-908, OW-908A, and OW-911A (Figure 7). These

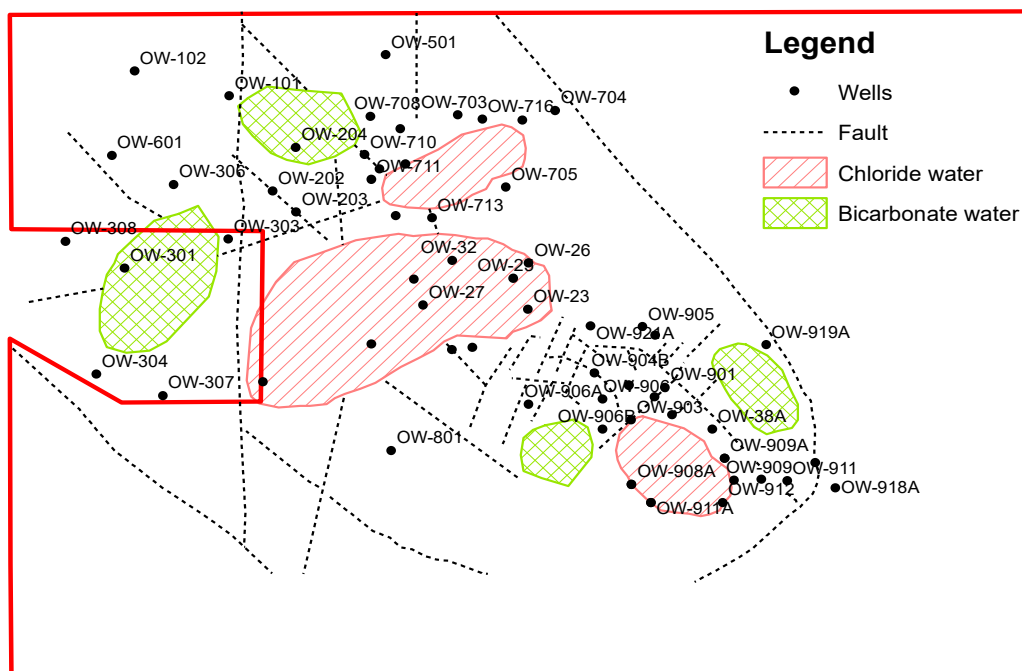


FIGURE 7: Distribution of two water types in the Olkaria geothermal area (KenGen, 2014)

areas are characterized by chloride-dominated fluids. Areas around wells OW-914 and OW-902 have peripheral waters and are thus thought to be on the margins of the reservoir.

The influence of structures is also apparent with the NW-SE trending faults being associated with high temperatures and chloride-rich waters. The NE-SW trending faults tend to carry cold waters that have led to a decline in enthalpies in the wells OW-719, OW-32, and OW-16 where they cut through (Wamalwa et al., 2014). Wamalwa et al., (2014) added that the faults within the Ol Njorowa gorge (between the Olkaria East and Olkaria Domes) carry cold, less mineralized water that tend to dilute the wells in the shallow depths as can be seen in the cases of wells OW-21, OW-22, and OW-23.

4. METHODOLOGY

4.1 Sampling and analysis

This study comprises samples from four producing wells of three fields out of seven in the Olkaria geothermal area (Table 1). The sampling and analysis was carried out by KenGen staff using methods as described by Arnórsson et al. (2006) and Stefansson et al. (2007). The liquid and vapour phases were separated using a Webre separator connected to a pipeline. Care had to be taken to make sure that no condensation occurred as the fluid cools while running through the pipeline on its way in and out of the separator. After the setup, vapour samples were collected into pre-evacuated gas bulbs (100 ml) containing 40% NaOH. CO₂, and H₂S were absorbed in the NaOH solution while the non-condensable

TABLE 1: Geochemical data from the studied wells

	OW-44	OW-724A	OW-914	OW-915
WHP (bar-g)	14	10	11	11.58
SP (bar-g)	14	9	10	10
pH at 20°C	7.91	9.43	9.91	9.93
Enthalpy (KJ/Kg)	2500	1698	2111	2034
Cond ($\mu\Omega/cm$)	6130	2770	7482	2690
TDS (ppm)	3064	1660	3742	1345
SiO ₂ (ppm)	487	610	636	682
B (ppm)	14.41	3.783	2.37	3.17
Cl (ppm)	1203	452.7	431.54	480.64
F (ppm)	79	35.8	244.28	187.41
SO ₄ (ppm)	143.1	201.6	68.5	16.1
CO ₂ (ppm)	88.22	321.86	1520.6	246.62
H ₂ S (ppm)	0.15	7.14	6.3	17.88
Li (ppm)	1.83	1.42	2.547	0.671
Na (ppm)	827	508.7	1455	653.5
K (ppm)	245.9	70.95	445.9	189.8
Ca (ppm)	1.266	2.159	0.01	2.672
Mg (ppm)	0.54	0.033	1.282	0.047
Fe (ppm)	1.37	0.265	1.35	1.35
CO ₂ (mmol/100moles.H ₂ O)	88.4	261.3	498.1	329.8
H ₂ S (mmol/100moles.H ₂ O)	10.26	4.66	0.91	5.03
CH ₄ (mmol/100moles.H ₂ O)	0.29	0.03	0.61	0.25
H ₂ (mmol/100moles.H ₂ O)	12.91	9.62	12.26	19.5
N ₂ (mmol/100moles.H ₂ O)	21.21	12.15	18.05	2.58
O ₂ (mmol/100moles.H ₂ O)	0	0	0	0.35

WHP = well head pressure

SP = sampling pressure

gases, i.e. H₂, N₂, O₂, Ar and CH₄, became more concentrated in the gas-head of the gas bulb. The non-condensable gases were then analysed inside the head space of the gas bulbs using gas chromatography (GC) while the concentrations of CO₂ and H₂S were analysed in the alkaline condensate by titration. The liquid phase samples were cooled down using a stainless steel spiral that was connected to the Webre separator and immersed into a bucket of water. Samples used for major cation determination were filtered through 0.2 µm filters into polypropylene bottles and acidified with 0.5% HNO₃ and later analysed using an ion chromatography photometer (ICP). Samples used for major anion and CO₂ determination were also filtered through 0.2 µm filters into polypropylene and amber glass bottles and then analysed using ion chromatography (IC). The quality of the sampling and chemical analysis was ensured by using well-known standard solutions for calibration, running reference samples before starting the analysis and evaluation of charge balance for the analyses. The samples had a charge balance between -5 and +5%.

4.2 Data analysis

The chemical data was first run through SOLVEQ to determine the equilibrium state of the system and then through CHILLER analysing the processes that typically occur in most high-temperature fields (Reed et al., 2012a). These processes include boiling and condensing processes, fluid-fluid mixing and rocks titration (hydrothermal alteration of the mineralogy of a well as a result of hot fluids and rocks interaction).

4.2.1 Equilibrium evaluation

The equilibrium constants were determined using mineral assemblages that potentially control the concentrations of H₂S, H₂, and CO₂ in the aquifer fluid by using reactions as shown in Table 2 and temperature equations for the equilibrium constants in Table 3. These include thermodynamic data on oxide and silicate minerals as given by Holland and Powell (1990), data on sulfide minerals were adapted from a study published by Robie and Hemingway (1995). The thermodynamic properties of the dissolved gases were based on the solubility constants by Fernandez-Prini et al., (2003) and the standard Gibbs energies of the ideal gases given by Robie and Hemingway (1995). Considering the limited pressure range, the specific volume of minerals was assumed to be independent of temperature and pressure.

Activities of end-members in the epidote (epidote and clinozoisite), garnet (grossular and andradite), and prehnite (Al-prehnite and Fe-prehnite) solid solutions were used. The values were 0.8 and 0.2 for epidote and clinozoisite respectively as well as for Al and Fe-prehnite. Other minerals were used to have unit activity.

TABLE 2: Reaction equations for the equilibrium constants (Arnórsson et al., 2010)

1 H ₂ S:	$\frac{1}{3} \text{ pyrite} + \frac{1}{3} \text{ pyrrohtite} + \frac{2}{3} \text{ prehnite} + \frac{2}{3} \text{ H}_2\text{O} = \frac{2}{3} \text{ epidote} + \text{H}_2\text{S (aq)}$
2 H ₂ S:	$\frac{2}{3} \text{ grossular} + \frac{1}{3} \text{ pyrite} + \frac{1}{3} \text{ pyrrohtite} + \frac{2}{3} \text{ quartz} + \frac{4}{3} \text{ H}_2\text{O}$ $= \frac{2}{3} \text{ epidote} + \frac{2}{3} \text{ wollastonite} + \text{H}_2\text{S (aq)}$
3 H ₂ S:	$2 \text{ grossular} + \frac{1}{4} \text{ pyrite} + \frac{1}{2} \text{ magnetite} + 2 \text{ quartz} + 2\text{H}_2\text{O} = 2 \text{ epidote} + 2 \text{ wollastonite} + \text{H}_2\text{S (aq)}$
4 H ₂ S:	$\frac{1}{4} \text{ pyrite} + \frac{1}{2} \text{ pyrrohtite} + \text{H}_2\text{O} = \frac{1}{4} \text{ magnetite} + \text{H}_2\text{S (aq)}$
5 H ₂ :	$\frac{4}{3} \text{ pyrrohtite} + \frac{2}{3} \text{ prehnite} + \frac{2}{3} \text{ H}_2\text{O} = \frac{1}{4} \text{ magnetite} + \text{H}_2\text{S (aq)}$
6 H ₂ :	$\frac{2}{3} \text{ grossular} + \frac{4}{3} \text{ pyrrohtite} + \text{H}_2\text{O} = \frac{1}{4} \text{ magnetite} + \text{H}_2\text{S (aq)}$
7 H ₂ :	$6 \text{ grossular} + 2 \text{ magnetite} + 6 \text{ quartz} + 4 \text{ H}_2\text{O} = 6 \text{ epidote} + 6 \text{ wollastonite} + \text{H}_2 \text{ (aq)}$
8 H ₂ :	$\frac{3}{2} \text{ pyrrohtite} + \text{H}_2\text{O} = \frac{3}{4} \text{ pyrite} + \frac{3}{4} \text{ magnetite} + \text{H}_2 \text{ (aq)}$
9 CO ₂ :	$\text{Clinozoisite} + \text{Calcite} + \frac{3}{2} \text{ quartz} + \text{H}_2\text{O} = \frac{3}{2} \text{ prehnite} + \text{CO}_2 \text{ (aq)}$
10 CO ₂ :	$\frac{2}{5} \text{ Clinozoisite} + \text{Calcite} + \frac{3}{5} \text{ quartz} = \frac{3}{5} \text{ Grossular} + \frac{1}{5} \text{ H}_2\text{O} + \text{CO}_2 \text{ (aq)}$

TABLE 3: Log K-temperature equations for the reactions given in Table 2 above (Arnórsson et al., 2010)

1 $\log \text{H}_2\text{S}$	$13.608 + \frac{592324}{T^2} - \frac{9346}{T} - 0.043552T + 0.000029164T^2 + 5.139\log T$
2 $\log \text{H}_2\text{S}$	$13.659 + \frac{555082}{T^2} - \frac{9256.6}{T} - 0.043608T + 0.000028613T^2 + 5.148\log T$
3 $\log \text{H}_2\text{S}$	$-0.836 - \frac{216659}{T^2} - \frac{2847.3}{T} - 0.008524T + 0.00002366T^2 + 0.152\log T$
4 $\log \text{H}_2\text{S}$	$13.589 + \frac{590215}{T^2} - \frac{9024.5}{T} - 0.044882T + 0.000029780T^2 + 5.068\log T$
5 $\log \text{H}_2$	$-1.640 - \frac{124524}{T^2} - \frac{777.19}{T} - 0.0005501T + 0.00007756T^2 + 0.565\log T$
6 $\log \text{H}_2$	$-1.544 - \frac{151109}{T^2} - \frac{752.389}{T} - 0.0005868T + 0.00007080T^2 + 532\log T$
7 $\log \text{H}_2$	$1.444 - \frac{273812}{T^2} - \frac{3962.1}{T} - 0.002401T + 0.00001304T^2 + 0.979\log T$
8 $\log \text{H}_2$	$-1.654 - \frac{95456}{T^2} - \frac{621.84}{T} - 0.001257T + 0.00007569T^2 + 0.600\log T$
9 $\log \text{CO}_2$	$-0.890 - \frac{7251.5}{T^2} - \frac{1710.6}{T} - 0.004188T + 0.00002683T^2 + 0.640\log T$
10 $\log \text{CO}_2$	$-1.449 - \frac{40536}{T^2} - \frac{2135.9}{T} - 0.0065639T + 0.00002725T^2 + 0.193\log T$

T = Temperature in Kelvin

4.2.2 Evaluation of gas concentrations versus the reservoir processes

a. Gas concentrations as a result of boiling and condensing processes

The calculations were done according to Reed et al., (2012a, b). As an input the reservoir temperatures as calculated by the SOLVEQ software were used. CHILLER was run using the specified reservoir temperatures TEMP and a limit SLIM was set in a way that no temperature increments take place. The fluid pressures (PFLUID) in the pickup file was set lower than the saturation pressures while the temperature increments (STEP INCREM) for temperatures were set to -10 (decreasing temperatures). It must be noted that the oversaturated minerals as read out with SOLVEQ were suppressed to minimize their masking of the convergence of the equations. CHILLER was then executed. The programme equilibrated using the gas phase and started boiling following STEP INCREM temperature drop and adjusted PFLUID. Considering that the enthalpy (ENTH) was set at zero, CHILLER sets the current ENTH to be equal to the enthalpy of the aqueous phase at the given temperature. To ensure that the boiling process remained iso-enthalpic, the starting total enthalpy SENTH was set to zero and CHIM sets SENTH equal to the current total enthalpy ENTH. From the output (CHIMOUT.DAT, at full equilibration) the gas saturation was determined.

b. Fluid-fluid mixing ('Coolbrew' calculations)

This study first considered the mixing of aqueous solution inside a high temperature reservoir with enthalpy constraint scenario (Reed et al., 2012b). CHILLER computed the enthalpy balance between the boiling solution and the mixer solution. The change of composition of the system TOTAL MOLES was calculated as TOTAL MOLES + STEP INCREM * MIXER TOTAL MOLES while the total current enthalpy of the system was also changed from ENTH to ENTH + STEP INCREM * MIXER TOTAL MOLES * ENTHW (enthalpy of the mixer solution). The mixing first resulted in condensation of the gas phase at a constant temperature. As in the boiling evaluation, oversaturated minerals as read out with SOLVEQ were suppressed. According to Reed et al., (2012b) once the gas phase was condensed, CHILLER proceeded in computing fluid-fluid mixing and temperature change by setting TEMPC to a non-zero value. This allowed CHILLER to titrate a mixer solution of composition given by MIXER TOTAL MOLES into the current solution of a composition given by TOTAL MOLES. The composition of the mixer solution was in moles, except for water where MIXER TOTAL MOLES, was given in kilograms.

c. Water-rock interaction (MINSOLV option)

The water-rock interaction option in CHILLER option was enabled with MINSOLV being set to a non-zero value and allowing SiO_2 , Fe_2O_3 , FeO , MgO , CaO , Na_2O , FeS , and NaCl as reactants. CHILLER

then read the names and amounts of reactants specified in the CHIMRUN file and their stoichiometries from the MINOX data file (Reed et al., 2012b). At the start of a reaction calculation, the TOTAL MIXER was set to zero while the composition of the system changed from TOTAL MOLES to TOTAL MOLES + STEP INCREM * WTPC * 0.01 * SPEC/MVOX, where SPEC is the molar amount of a given component species in the reactant NOMOX. MVOX is the molecular weight of reactant NOMOX. For increments in moles, TOTAL MOLES are changed to TOTAL MOLES + STEP INCREM*WTPC*0.01*SPEC.

4.2.3 Evaluation of depth of gas breakout or bubble point

Gas breakout or two-phase conditions occur at a depth at which the gas pressure plus water pressure exceeds the total pressure, i.e. bubble point depth (Haizlip et al., 2012). In this case, the gas pressure is given in the output files of the CHIM programme whereas the water pressures were estimated using steam tables as follows:

$$P_{liq} = P_{wateratsatT} \quad (1)$$

$$P_{tot} = P_{gas} + P_{liq} \quad (2)$$

Where P_{liq} = pressure of the liquid phase in the well
 $P_{wateratsatT}$ = pressure of the saturated water at a given temperature
 T = temperature in kelvin
 P_{gas} = pressure of the gas phase in the well
 P_{tot} = total pressure

The temperature values were taken from the SOLVEQ output files and assigned to the major feed zones as determined from the downhole temperature and pressure profiles of each well as shown in Table 4.

5. RESULTS

The results are categorized into two parts. In part one the evaluation of the equilibrium states of the fluids in the wells is presented. In part 2 the processes leading to gas evolution are discussed. The results are visualized in gas pressure (bars) vs temperature graphs.

5.1 The equilibrium state of the fluids

The logH₂ vs temperature curve (Figure 8) is defined by Equations 5, 6, 7 and 8 in Table 2. The studied wells closely correlate mineral assemblages in Equation 5 which are pyrrhotite, prehnite, epidote, and pyrite, and 8 with magnetite, pyrite and pyrrhotite (Table 4). Wells OW-44 and OW-914 appear to be closest to equilibrium. Wells OW-915 and OW-724A are in equilibrium as they plot far from the top most curve (Equation 5). These results agree with those by Arnórsson et al., (2010) where some wells in the field plotted close to the mineral assemblages in 5 and 8 indicating equilibrium with the minerals while others were scattered hence showing non-equilibrium. The gas concentration is low, ranging between -2.0 moles/kg in well OW-915 and -2.5 moles/kg in well OW-914 which closely corresponds to a range between -3 moles/kg to -5.5 moles/kg (Arnórsson et al., 2010).

In the log H₂S vs temperature graph there are mineral curves for 1, 2, 3 and 4 (Figure 9). The wells range between 300°C and 330°C, except for well OW-724A that lies at 250°C. Well OW-724A seems to be in equilibrium with mineral assemblage in Equation 1 which describes the ratio of pyrite, pyrrhotite, prehnite and epidote and 4 (pyrite, pyrrhotite and magnetite). Well OW-44, on the other hand, fits to the mineral assemblages grossular, pyrite, pyrrhotite, quartz, epidote and wollstonite (Equation 2) and grossular, pyrite, magnetite, quartz, epidote and wollastonite (Equation 3). Wells OW-

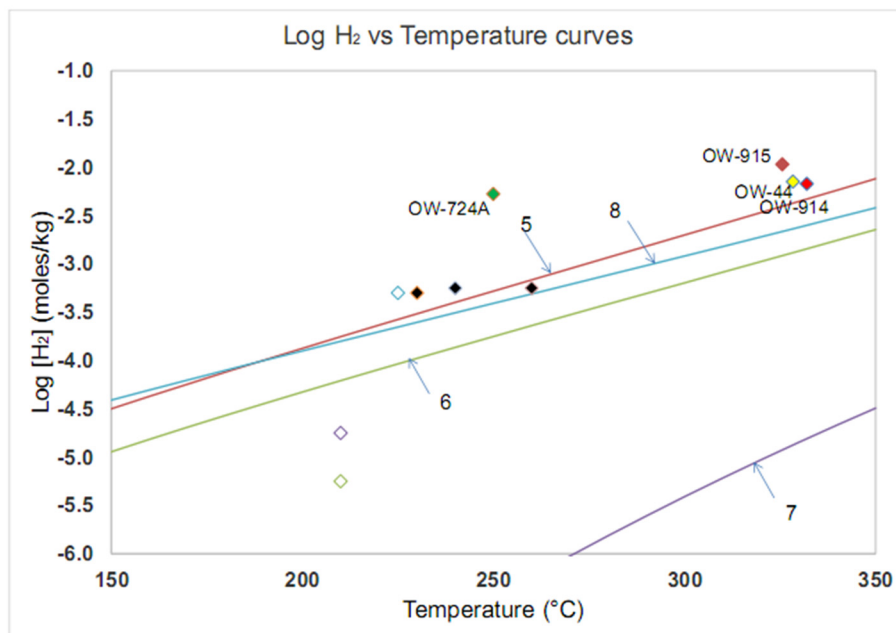


FIGURE 8: Calculated concentrations of H₂ in the total aquifer fluid of wells OW-44, OW-724A, OW-914, and OW-915. White and black symbols are data from Arnórsson et al., (2010) of the Olkaria Domes and Olkaria Central field respectively. The numbers on the curves refer to the reactions in Table 2

915 and OW-914 seems not to be in equilibrium with any of the mineral assemblages. The results still hold for Arnórsson et al., (2010) with the exception of well OW-914 which seemed depleted with H₂S, an indication of steam loss and therefore gas loss. The log CO₂ graph (Figure 10) is defined by two mineral assemblages 9 and 10. Two wells, i.e., OW-914 and OW-915 are in equilibrium with mineral assemblage given by Equation 10. Well OW-44 plots way below the mineral assemblage in Equation 9 whereas well OW-724A plots above the mineral assemblage in Equation 10. This is an indication that

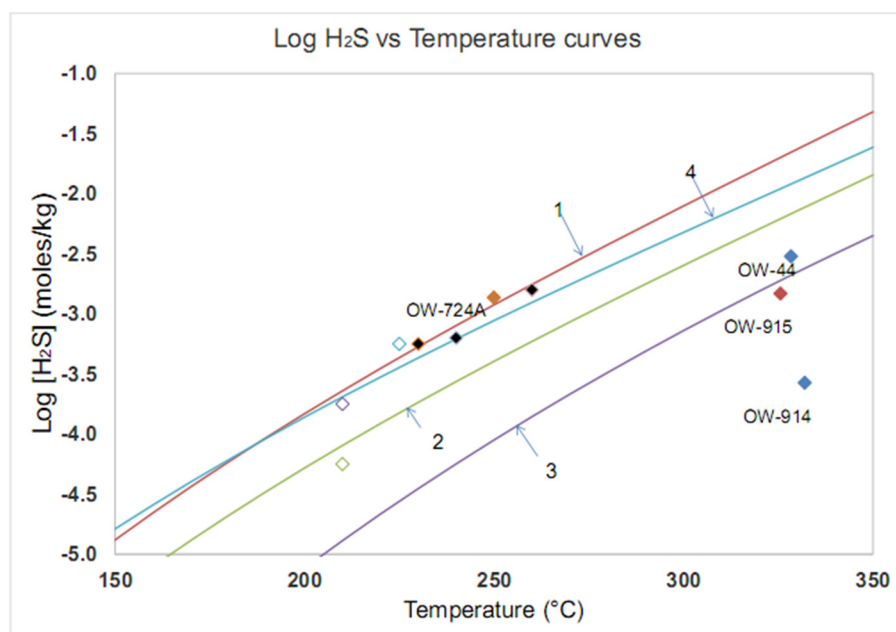


FIGURE 9: Calculated concentrations of H₂S in the total aquifer fluid of wells OW-44, OW-724A, OW-914, and OW-915. White and black symbols are Arnórsson et al., (2010) data from Olkaria Domes and Olkaria Central field respectively. The numbers on the curves refer to the reactions in Table 2

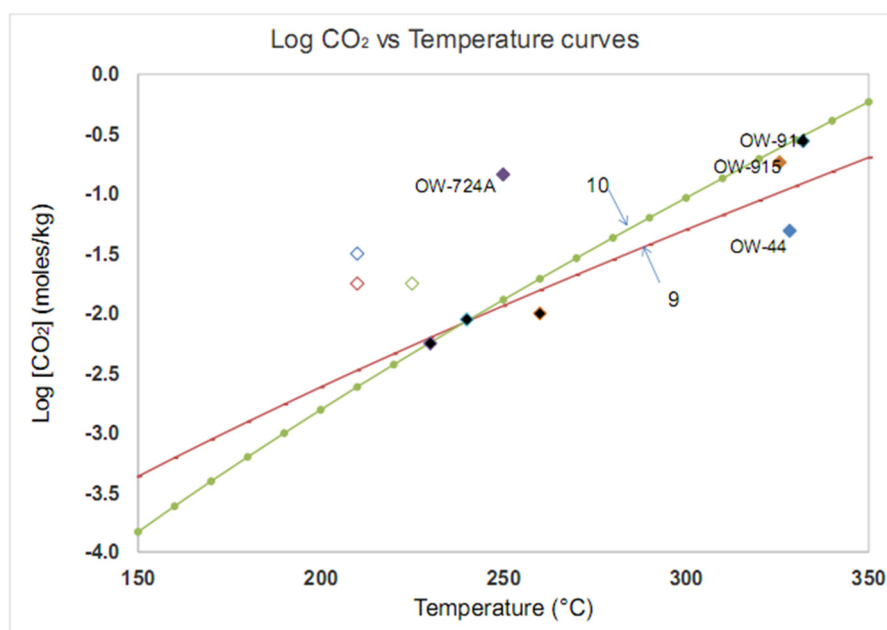


FIGURE 10: Calculated concentrations of H_2 in the total aquifer fluid of wells OW-44, OW-724A, OW-914, and OW-915. White and black symbols are Arnórsson et al., (2010) data from Olkaria Domes and Olkaria Central field respectively. The numbers on the curves refer to the reactions in Table 2

well fluids in OW-724A and OW-44 are not in equilibrium with the mineral assemblages. The values of concentration also suggest that well OW-44 has the smallest amount of gas whereas well OW-914 has the highest. The findings concur with Arnórsson et al., (2010) where the Domes Sector has the highest CO_2 concentration what is likely caused by the high flux of it from the heat source.

5.2 Gas concentrations and the reservoir processes in the wells

The analysed reservoir processes are boiling, fluid-fluid mixing and titration (Figures 11-14). The plots for well OW-44 indicate that boiling is the major process leading to evolution of gases. The gas pressures increased with temperature, steadily rising from 2.4 to 50 bars. The mixing process is the second most dominant. Unlike the boiling process, the curve remains stable up to about 200°C before starting to increase. The curve on titration has almost similar trend but smaller values ranging between 0 and 2.4 bars (Figure 11).

For well OW-724A, just like well OW-44 boiling is the major process leading to gas evolution (Figure 12). Between 100°C and 120°C the gas pressure is constant at about 0.1 bars before steadily rising up to 37 bars. The mixing curve also experiences no change in the gas pressures at low temperatures but later increases. The recorded values are with 0.1 and 17 bars smaller than those related to the boiling processes. The titration process start with a linear increase in the gas pressures up to around 180°C. The curve then shows a decline in the gas pressures between 180°C and 220°C.

Caused by boiling, the resulting gas pressures in well OW-914 are ranging between 10 and 92 bars (Figure 13). The values of the mixing curve range between 0 and 50 bars. The titration curves show almost no increase between 100°C and 200°C. This is followed by a slight increase to about 2.5 bars at 300°C. In well OW-915 just like in OW-914 the gas pressures reach a maximum pressure of 85 bars as a consequence of the boiling process (Figure 14). The mixing curve shows a slight increase in gas pressure with temperature, the values lie between 0 and 10 bars. The titration curve shows similar trends as well OW-724A. The curve starts with an increase in gas pressures up to a temperature of 170°C, plateaus until 210°C before starting to increase again to 5 bars.

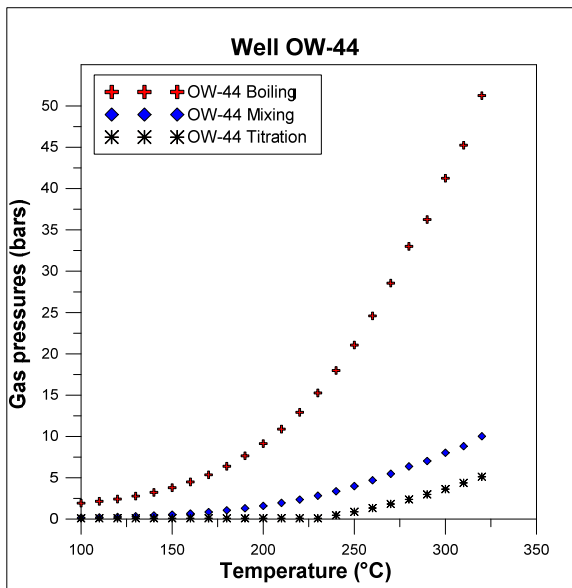


FIGURE 11: Gas pressures against the reservoir processes in well OW-44

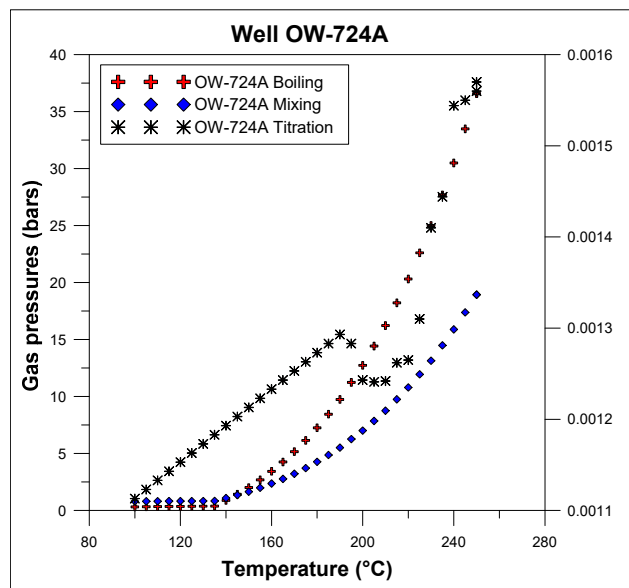


FIGURE 12: Gas pressures against the reservoir processes in well OW-724A. The titration curve has been plotted on the secondary axis

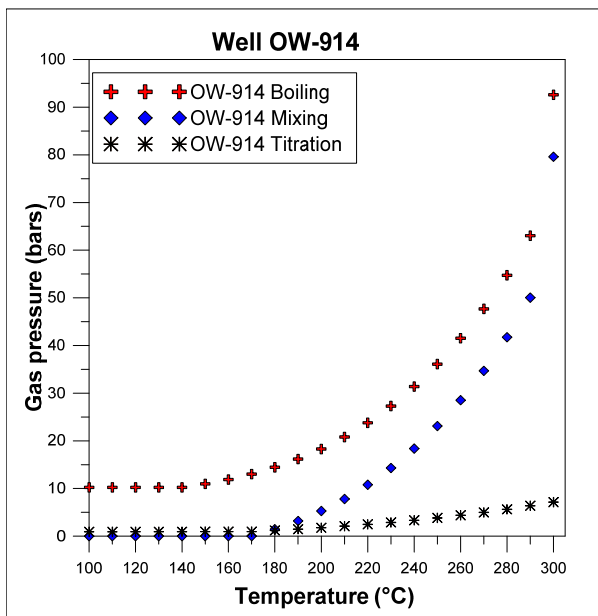


FIGURE 13: Gas pressures against the reservoir processes in well OW-914

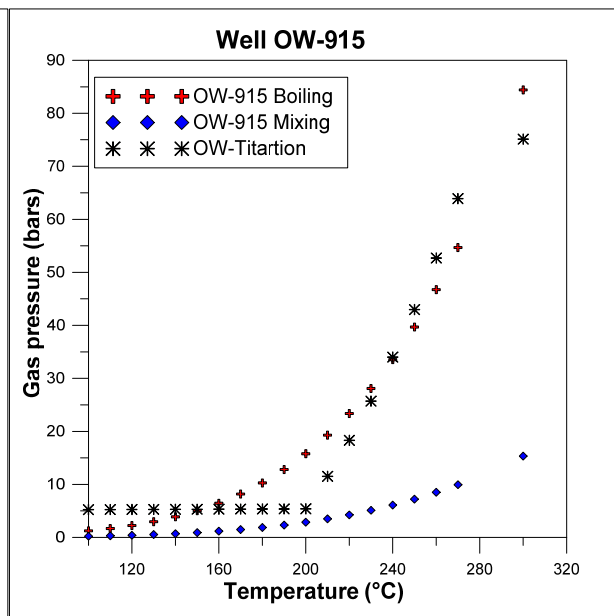


FIGURE 14: Gas pressures against the reservoir processes in well OW-915

The process comparison curves (Figure 15) indicate boiling processes to be the most dominant process in well OW-914 followed by OW-915 and OW-724A. Well OW-44 has the smallest gas pressures generated. Gas evolution caused by mixing processes on the other hand, seems high in well OW-914 followed by OW-724A, OW-915, and OW-44. Titration processes as well as mixing processes produce higher values in OW-914. Well OW-915 comes in second followed by OW-44 and OW-724A.

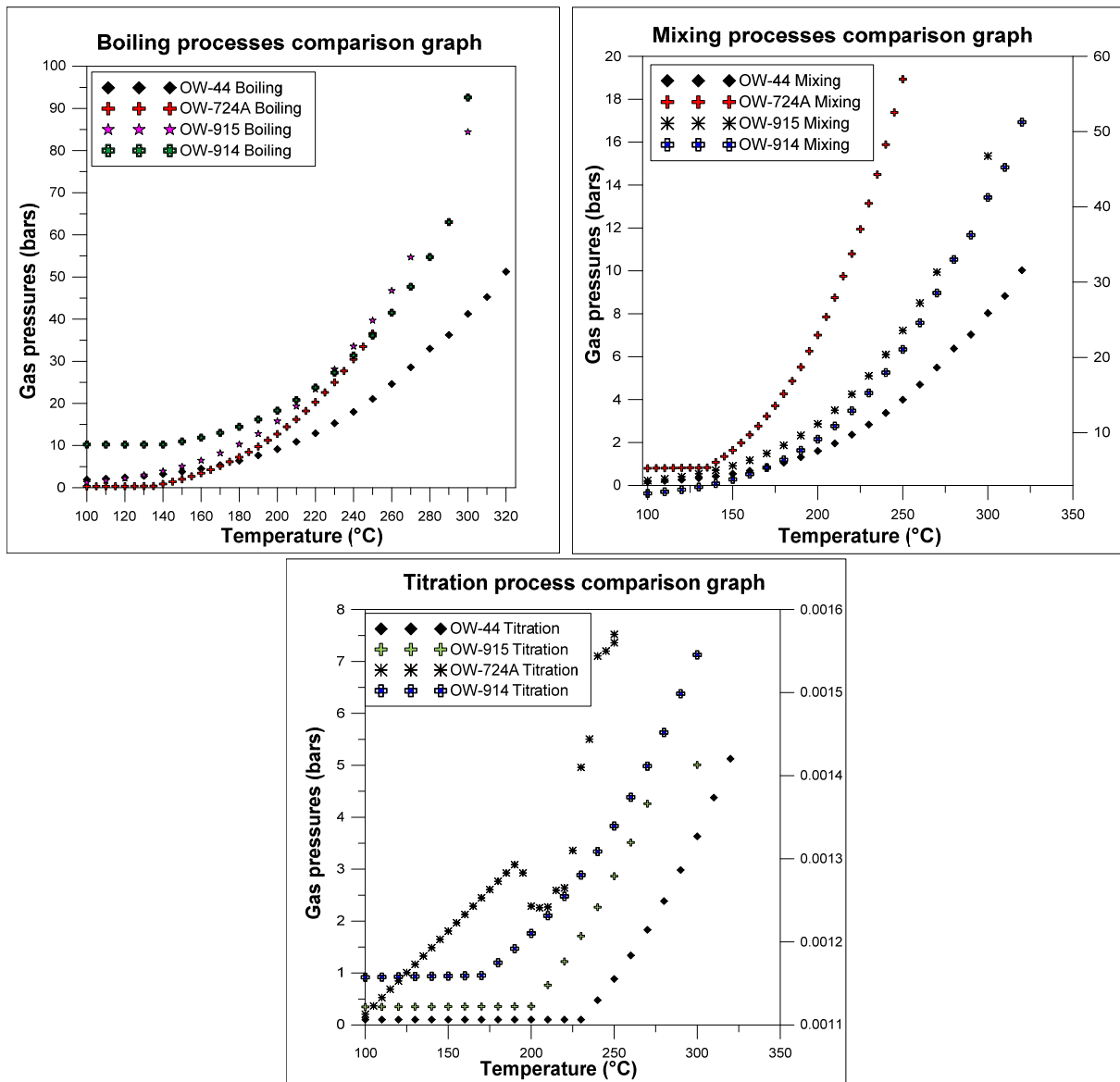


FIGURE 15: Reaction processes comparison graphs. The titration curve in well OW-724A has been plotted on the secondary axis

5.3 Depth of gas breakout or bubble point

The measured pressures at the major feed zones reach the highest values with 175 bars in well OW-44 followed by OW-915 with 150 bars, OW-914 with 100 bars and OW-724A with 90 bars (Table 4). Using steam tables, liquid and gas pressure (P_{liquid} and P_{gas} from CHIM) are added. The total values range between 52 bars in OW-44 and 92 bars in the OW-914. Well OW-914 has a total pressure close to the pressure measured downhole, indicating higher probability of gas break out at its major feed zone. Well OW-44 had the smallest probability, as its total pressure is with 52 bars much lower than the 175 bars that were measured.

TABLE 4: A comparison between measured and calculated pressures in the main feed zones

Well name	Depth of major feed zone (m)	Measured pressure (bars)	Calculated liquid pressure (bars)	Calculated gas pressure (bars)	Total calculated pressure (bars)
OW-44	2250	175	0.105	52	52
OW-724A	1700	90	0.002	36	36
OW-914	1500	100	0.025	92	92
OW-915	2300	150	0.035	84	84

6. DISCUSSION OF THE RESULTS

6.1 The equilibrium state of the fluids

This study and the one of Arnórsson et al., (2010) agree that the H₂ and H₂S gas concentrations are low in the Olkaria geothermal field. This is indicated by small concentration values ranging between -2 to -3.5 moles/kg (Figure 8 and 9) indicating that the aquifer vapour fraction is insignificant. Arnórsson et al., (2010) attribute these low concentrations to steam loss resulting from the boiling of fluid flowing into these wells. Well OW-724A shows values way above the mineral assemblage curves of H₂ whereas well OW-914 is below the H₂S graph. According to Arnórsson et al., (2010), non-equilibrium distributions of gas species in a high temperature field like Olkaria arises from processes like boiling, condensation and mixing.

The CO₂ plot indicates that the calculated aquifer fluid CO₂ concentrations are in equilibrium with mineral assemblages as seen in the case of well OW-914 and OW-915. Well OW-44, apart from being in non-equilibrium with the mineral assemblages, has the smallest concentration (Figure 10). According to Arnórsson et al., (2010), the low CO₂ values as found in well OW-44 are due to an insufficient supply of the gas into the fluid preventing it from saturating with calcite. This shows that the aquifer fluid CO₂ concentration is externally controlled indicating, that the flux into the geothermal fluid originates either from degassing magma or from fluid- and/or fumaroles-rock interaction. This is opposite to the case of well OW-724A which is higher than the equilibrium curves. It supports the possibility that the non-equilibrium in well OW-724A maybe a result of a volcanic degassing process underneath these areas but with minor gas loss compared to OW-44.

6.2 Gas concentrations and the reservoir processes in the wells

The results point to boiling being the major process which leads to evolution of gases (Figures 11-14). Simsek et al., (2009) who were studying the Kizildere geothermal field in Turkey stated that the increase in gases is a result of elevated enthalpy. This is thought to be a consequence of flow or gravity segregation of water. The percentage of water in the reservoir increases either due to a decrease of steam which flows to the well or enhanced vaporization boiling when there is heat flow from the rock into the fluid. The former process describes a scenario of boiling in the area around the well while the second becomes dominant if the water has cooled by adiabatic boiling as a result of pressure drop which leads to steam and gas generation (Simsek et al., 2009). From the graph, it is notable that the intensity of the processes increases with temperatures in the wells in question. Temperature act as catalyst for reactions leading to evolution of the gases (Haizlip et al., 2012).

A comparison of magnitude of these processes indicates that the impacts of the processes are highest in well OW-914 and lowest in OW-44 (Figure 15). This trend in well OW-914 is attributed to the high temperature values of about 325°C in a way that chain reactions similar to those discussed in the mixing processes take place. This is further supported by the fact that this well has high injectivity index of

about 315 l pm/bar, an indication of high permeability in the rock surrounding the well. In streaming fluids react with the mineral assemblages in the aquifer rocks that leads to the evolution of gases.

Well OW-44 had the smallest gas concentrations resulting from the analysed reservoir processes despite the fact that it has high downhole temperatures of about 300°C and considerably high injectivity index. Hazil et al, (2012) attribute this to loss of gas from the deep fluid as a consequence of degassing and near surface boiling. Besides that, NH₃, H₂, and H₂S can be removed from the steam, released by boiling, by processes such as wall-rock interactions and solution into steam condensate. Depending on how far the well is from the recharge zone, gases in the reservoir fluid tend to enter the vapour phase whenever possible (Simsek et al., 2009). Therefore, when boiling sets in, the initially formed steam contains a majority of the dissolved gases while the residual liquid is highly depleted in dissolved gases and later stages of steam separation will contain significantly lower concentrations of gases. Steam formed in the early stages of boiling is characterized by a higher gas content.

6.3 Depth of gas breakout or bubble point

One aim of this study is to determine the potential impacts of gases on the performance of the wells. The results (Table 4) indicate that the probability of a gas breakout is highest in well OW-914 and lowest in OW-44. This is an indication that well OW-914 is likely to experience calcite scaling at its major feed zone at 1500 m depth, considering the type of waters feeding the well. This finding agrees with a dynamic survey carried out in OW-914 well in 2014 (Figure 16) where a calcite scaling potential in the depths between 1200 and 1800 m was indicated. According to Akin et al. (2015), thermal fluids rising in a wellbore experience boiling and degassing of CO₂ as a consequence of pressure drop.

When the initial gas bubbles are formed, CO₂ exsolution affects the pH together with the carbonate species leading to the thermal fluid becoming saturated in respect to calcite.

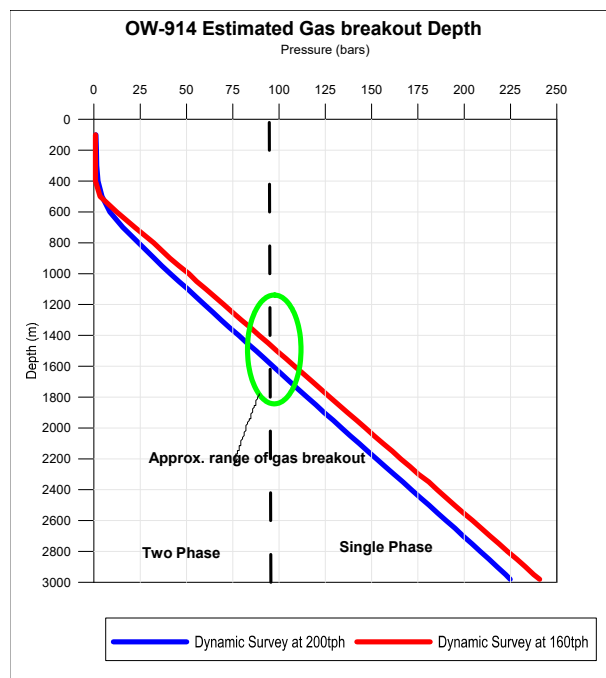


FIGURE 16: Estimated gas breakout depth in well OW-914 from the dynamic surveys

7. POSSIBLE RESERVOIR MANAGEMENT OPTIONS

Continuous exploitation tends to increase the concentration of non-condensable gases in the reservoir (Moya and Yock, 2005). The same study emphasizes the need to establish a program for detailed monitoring of the non-condensable gases at each well in order to determine the principal causes of the increase. The best injection and production strategies have to be found to improve the existing operating conditions.

This study points to the conclusion that the principal cause of the increase in non-condensable gases is a pressure decline in the reservoir consequently leading to depressurization boiling. In order to minimize this tendency, two different strategies for the different parts of the Olkaria geothermal field were considered (Figure 17). Firstly, a reinjection programme which will help to increase the volume of fluids injected in the eastern sector (suitable for example for well OW-44). The immediate response here would be a decrease in the enthalpy of the wells and gases evolution.

For wells with similar chemistry as well OW-914, two options are applicable. The first is the operation of the wells at a flow rate near the minimum. According to Moya and Sanchez (2005) this will minimise pressure drop and consequently non-condensable gas evolution due to depressurization boiling. This will consequently lead to a lowered scaling potential and/or reduced numbers of work overs in case scaling occurs. The second option will be to rethink the chemical dosage. According to Haizlip et al., (2012) successful scale mitigation in the wellbore requires that the inhibitor is injected into the flowing well through capillary tubing at depths 10-50 m below the estimated gas breakout depth preferably within the casing. The inhibitors prevent the growth of scale.

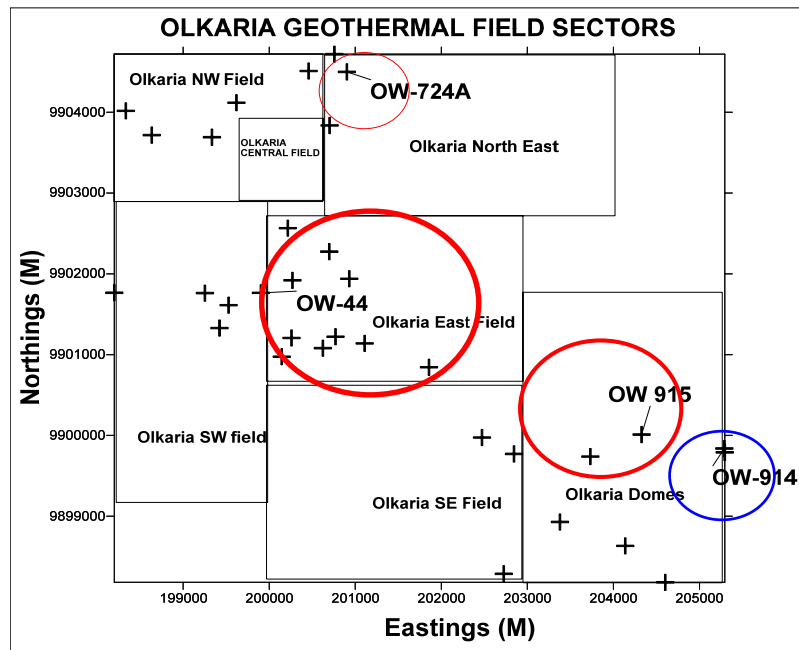


FIGURE 17: Management options for different parts of the field.; red eclipses stand for reinjection while the blue one is for reduced flow from wells and inhibition

The inhibitors prevent the growth of scale.

8. CONCLUSIONS

The study concludes that:

- The gas species are not in equilibrium with the mineral assemblages due to processes of boiling, condensation, and mixing. The wells OW-914 and OW-915 are exceptions which are in equilibrium with mineral assemblages given by Equation 10;
- The CHILLER evaluation shows boiling as the major process leading to the evolution of gases;
- Well OW-44 had the smallest gas concentrations arising from the considered reservoir processes due to degassing and near surface boiling;
- Gas breakout is most likely in well OW-914 and least in OW-44;
- Different strategies for the management of different parts of the Olkaria geothermal field can be used. One option is increased volume of fluids injected in the eastern sector (for example in well OW-44). The second option, which is suitable for OW-914, is to operate the wells at a minimum flow rate or the use of chemical inhibitors.

ACKNOWLEDGEMENTS

Completion of this work is attributed to support received from various sources which I wish to sincerely thank. First and foremost, to my Almighty God for his grace, faithfulness and guidance that enabled me to cope with challenges of academic life. Sincere gratitude to the entire UNU-GTP fraternity and more so to my supervisor Tobias Weisenberger for his continuous guidance throughout the research. I am greatly indebted to the Kenya Electricity Generating Company LTD (KenGen) for supporting my entire study through finances, lab facilities and permission to use the data. I wish to acknowledge the contributions made by the Geochemistry team through data collection.

REFERENCES

- Akin, T., Guney, A., and Kargi, H., 2015: Modeling of calcite scaling and estimation of gas breakout depth in a geothermal well by using PHREEQC. *Proceedings of the Fortieth Workshop on Geothermal Reservoir Engineering, Stanford University, Stanford, CA, United States*, 8 pp.
- Ambusso, W.J. and Ouma, P.A., 1991: Thermodynamic and permeability structure of Olkaria Northeast field: Olkaria fault. *Geothermal Resource Council, Transactions, 15*, 237-242.
- Angcoy, E.C., 2010: *Geochemical modelling of the high-temperature Mahanagdong Geothermal Field, Leyte, Philippines*. University of Iceland, MSc thesis, UNU-GTP, Iceland, report 1, 71 pp.
- Arnórsson, S., Angcoy, E.C., Bjarnason, J.Ö., Giroud, N., Gunnarsson, I., Kaasalainen, H., Karingithi, C., and Stefánsson, A., 2010: Gas chemistry of volcanic geothermal systems. *Proceedings of the World Geothermal Congress 2010, Bali, Indonesia*, 12 pp.
- Arnórsson, S., Bjarnason, J.Ö., Giroud, N., Gunnarsson, I., and Stefánsson, A., 2006: Sampling and analysis of geothermal fluids. *Geofluids, 6*, 203-216.
- Ármannsson, H., 2003: CO₂ emission from geothermal power plants. *Proceedings of the International Geothermal Conference IGC-2003 "Multiple Integrated Uses of Geothermal Resources" Reykjavík, Session 12*, 56-62.
- Bienkowski, R., Torres-Alvarado, I.S. and Hinderer, M., 2003: *Genese hochsaurer Fluide im Geothermalfeld von Los Humeros, Zentral-Mexiko*. Institut für Angewandte Geowissenschaften, Technische Universität Darmstadt, Diplomarbeit (MSc thesis in German), 89 pp.
- Clarke, M.C.G., Woodhall, D.G., Allen, D., and Darling, G., 1990: *Geological, volcanological and hydrogeological controls of the occurrence of geothermal activity in the area surrounding Lake Naivasha, Kenya*. Ministry of Energy, report, 138 pp.
- Fernandez-Prini, R., Alvarez, J.L., and Harvey, A.H., 2003: Henry's constants and vapor-liquid distribution constants for gaseous solutes in H₂O and D₂O at high temperatures. *J. Phys. Chem. Ref. Data, 32*, 903-916.
- Giroud, N., and Arnórsson, S., 2005: Estimation of long-term CO₂ and H₂S release during operation of geothermal power plants. *Proceedings of the World Geothermal Congress 2005, Antalya, Turkey*, 6 pp.
- Gudmundsson, B.T., and Arnórsson, S., 2002: Geochemical monitoring of the Krafla and Námafjall geothermal areas, N-Iceland. *Geothermics, 31*, 195-243.
- Haizlip, J.R., Guney, A., Tut Haklidir, F.S. and Garg, S.K., 2012: The impact of high non condensable gas concentrations on well performance – Kizildere geothermal reservoir, Turkey. *Proceedings of the 37th Workshop on Geothermal Reservoir Engineering, Stanford University, Stanford, CA, US*, 6 pp.
- Holland, T.J.B., and Powell, R., 1990: An enlarged and updated internally consistent thermodynamic dataset with uncertainties and correlations: K₂O-Na₂O-CaO-MgO-MnO-FeO-Fe₂O₃-Al₂O₃-TiO₂-SiO₂-C-H₂-O₂. *J. Metamorphic Petrology, 8*, 89-124.
- Karingithi, C.W., 2000: Geochemical characteristics of the Greater Olkaria geothermal field, Kenya. Report 9 in: *Geothermal training in Iceland 2000*. UNU-GTP, Iceland, 165-188.

Karingithi, C.W., 2002: *Hydrothermal mineral buffers controlling reactive gases concentration in the Greater Olkaria geothermal system, Kenya*. University of Iceland, MSc thesis, UNU-GTP, Iceland, report 2, 51 pp.

KenGen, 1999: *Conceptualized model of the Olkaria geothermal field*. Kenya Electricity Generating Company Ltd. (KenGen), internal report no. 10, 46 pp.

KenGen, 2014: *Revised geochemical model of the Olkaria geothermal field*. Kenya Electricity Generating Company Ltd. (KenGen), internal report no. 1, 23 pp.

Lagat, J., Arnórsson, S. and Franzson, H., 2005: Geology, hydrothermal alteration and fluid inclusion studies of Olkaria Domes Geothermal Field, Kenya. *Proceedings of the World Geothermal Congress 2005, Antalya, Turkey*, 14 pp.

Moya, P., and Sánchez, E., 2005: Non-condensable gases at the Miravalles geothermal field. *Proceedings of the 30th Workshop on Geothermal Reservoir Engineering, Stanford University, Stanford, CA, United States*, 11 pp.

Moya, P., and Yock, A., 2005: First eleven years of exploitation at the Miravalles geothermal field. *Proceedings of the Thirtieth Workshop on Geothermal Reservoir Engineering, Stanford University, Stanford, CA, United States*, 8 pp.

Mungania, J., 1992: *Preliminary field report on geology of Olkaria volcanic complex with emphasis on Domes area field investigations*. Kenya Power Company, internal report 11, 37 pp.

Naylor, W.I., 1972: *The geology of the Eburru and Olkaria geothermal projects*. United Nations Development Programme, report no. 01, 52 pp.

Ofwona, C.O., 2002: *A reservoir study of Olkaria East geothermal system, Kenya*. University of Iceland, MSc thesis, UNU-GTP, Iceland, report no. 1, 74 pp.

Ogoso-Odongo, M.E., 1986: Geology of Olkaria geothermal field. *Geothermics*, 15, 741-748.

Omenda, P.A., 1994: Geological control on the reservoir characteristics of Olkaria West Geothermal Field, Kenya. *Proceedings of the Nineteenth Workshop on Geothermal Reservoir Engineering, Stanford University, Stanford, CA, United States*, 125-129.

Omenda, P.A., 2000: Anatectic origin for comendite in Olkaria geothermal field, Kenya Rift; Geochemical evidence for syenitic protholith. *African J. Science and Technology*, 1, 39-47.

Ouma, P.A., 1999: *Reservoir engineering report for Olkaria Domes field*. Kenya Electricity Generating Company Ltd. (KenGen), internal report 14, 54 pp.

Reed, M.H., Spycher, N.F., and Palandri, J., 2012a: *SOLVEQ-XPT: A computer program for computing aqueous-mineral-gas equilibria*. University of Oregon, Department of Geological Sciences, Eugene, OR, United States, 43 pp.

Reed, M.H., Spycher, N.F., and Palandri, J., 2012b: *Users guide for CHIM-XPT: A program for computing reaction processes in aqueous-mineral-gas systems and MINTAB guide (Ver 2.43)*. University of Oregon, Department of Geological Sciences, Eugene, OR, United States, 73 pp.

Robie, R.A. and Hemingway, B.S., 1995: *Thermodynamic properties of minerals and related substances at 298.15 K and 1 bar (105 Pascals) pressures and at higher temperatures*. U.S. Geological Survey Bulletin, 2131, 461 pp.

Shackleton, R.M., 1986: Precambrian collision tectonics in Africa. In: Coward, M.P. and Ries, A.C. (editors), *Collision Tectonics*. Geological Society, London, United Kingdom, special publications 1986-19, 329-349.

Simsek, S., Parlaktuna, M. and Akın, S., 2009: *Data gathering and evaluation of Kizildere geothermal field*. Report for Zorlu Energy, 13 pp.

Smith, M. and Mosley, P., 1993: Crustal heterogeneity and basement influence on the development of the Kenya rift, East Africa. *Tectonics*, 12, 591-606.

Thompson, A.O. and Dodson, R.G., 1963: *Geology of the Naivasha area*. Geological Survey Kenya, report no. 55, 88 pp.

Virkir, 1980: *Geothermal development at Olkaria*. Virkir Consulting Group, report no. 09 prepared for Kenya Power Company, 40 pp.

Wamalwa, R., Nyamai, C.M., Ambusso, W. and Mulwa, J., 2014: Structural controls on the chemistry and output of the wells in the Olkaria geothermal field, Rift Valley, Kenya. *Proceedings of the 5th African Rift Geothermal (ARGeo-C5), Arusha, Tanzania*, 11 pp.

Wambugu, J.M., 1995: *Geochemical update of Olkaria West geothermal field*. Kenya Power Company Ltd., internal report no. 5, 40 pp.

West JEC, 2009: *The Olkaria optimization study (Phase II) – Final reservoir analysis report*. West Japan Engineering Consultants Inc., 301 pp.